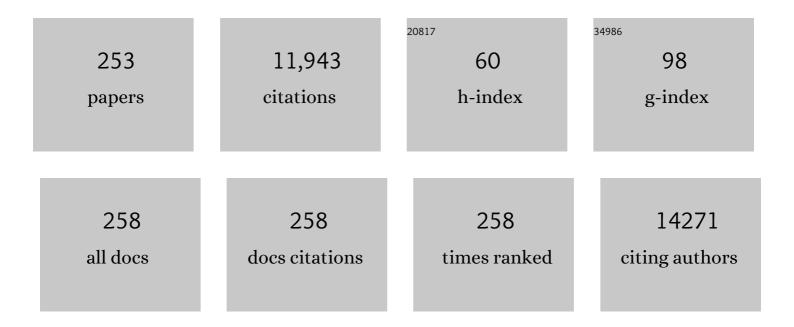
Stefan Vogt

List of Publications by Year in descending order

Source: https://exaly.com/author-pdf/6240308/publications.pdf Version: 2024-02-01



STEEAN VOCT

#	Article	IF	CITATIONS
1	Dynamic zinc fluxes regulate meiotic progression in <i>Caenorhabditis elegans</i> . Biology of Reproduction, 2022, 107, 406-418.	2.7	5
2	Broadband X-ray ptychography using multi-wavelength algorithm. Journal of Synchrotron Radiation, 2021, 28, 309-317.	2.4	20
3	Development of Fe3O4 core–TiO2 shell nanocomposites and nanoconjugates as a foundation for neuroblastoma radiosensitization. Cancer Nanotechnology, 2021, 12, 12.	3.7	9
4	Use of X-Ray Fluorescence Microscopy for Studies on Research Models of Hepatocellular Carcinoma. Frontiers in Public Health, 2021, 9, 711506.	2.7	1
5	Achieving high spatial resolution in a large field-of-view using lensless x-ray imaging. Applied Physics Letters, 2021, 119, .	3.3	15
6	Development of Multi-Scale X-ray Fluorescence Tomography for Examination of Nanocomposite-Treated Biological Samples. Cancers, 2021, 13, 4497.	3.7	4
7	Ptychopy: GPU framework for ptychographic data analysis. , 2021, , .		1
8	Three-dimensional reconstruction of integrated circuits by single-angle X-ray ptychography with machine learning. , 2021, , .		0
9	Method development of X-ray ptychography: Towards high-resolution and high-throughput coherent imaging. , 2021, , .		Ο
10	Multi-beam X-ray ptychography for high-throughput coherent diffraction imaging. Scientific Reports, 2020, 10, 19550.	3.3	10
11	Measurement of moisture-dependent ion diffusion constants in wood cell wall layers using time-lapse micro X-ray fluorescence microscopy. Scientific Reports, 2020, 10, 9919.	3.3	18
12	High-speed Three-dimensional Imaging at the Nanoscale via Fly-scan Ptycho-tomography. Microscopy and Microanalysis, 2020, 26, 1006-1008.	0.4	0
13	Fungal–copper interactions in wood examined with large field of view synchrotron-based X-ray fluorescence microscopy. Wood Material Science and Engineering, 2019, 14, 174-184.	2.3	6
14	X-ray methods to observe and quantify adhesive penetration into wood. Journal of Materials Science, 2019, 54, 705-718.	3.7	28
15	Copper distribution and oxidation states near corroded fasteners in treated wood. SN Applied Sciences, 2019, 1, 1.	2.9	6
16	The Velociprobe: An ultrafast hard X-ray nanoprobe for high-resolution ptychographic imaging. Review of Scientific Instruments, 2019, 90, 083701.	1.3	61
17	Correlative 3D X-ray Fluorescence and Ptychographic Tomography of Frozen-Hydrated Green Algae. Microscopy and Microanalysis, 2019, 25, 114-115.	0.4	0
18	Correlative X-ray Ptychographic and Fluorescence Imaging at the Advanced Photon Source. Microscopy and Microanalysis, 2019, 25, 1030-1031.	0.4	1

#	Article	IF	CITATIONS
19	High-speed and Large Field-of-view Imaging via X-ray Fly-scan Ptychography. Microscopy and Microanalysis, 2019, 25, 46-47.	0.4	1
20	Copper Transporter ATP7A (Copper-Transporting P-Type ATPase/Menkes ATPase) Limits Vascular Inflammation and Aortic Aneurysm Development. Arteriosclerosis, Thrombosis, and Vascular Biology, 2019, 39, 2320-2337.	2.4	28
21	Bovine eggs release zinc in response to parthenogenetic and sperm-induced egg activation. Theriogenology, 2019, 127, 41-48.	2.1	34
22	Instrumentation and method developments of x-ray ptychography at the Advanced Photon Source. , 2019, , .		3
23	Optimization-based simultaneous alignment and reconstruction in multi-element tomography. Optics Letters, 2019, 44, 4331.	3.3	8
24	Optimized illumination for high-throughput ptychography. , 2019, , .		0
25	Quantifying X-Ray Fluorescence Data Using MAPS. Journal of Visualized Experiments, 2018, , .	0.3	16
26	Investigation into the intracellular fates, speciation and mode of action of selenium-containing neuroprotective agents using XAS and XFM. Biochimica Et Biophysica Acta - General Subjects, 2018, 1862, 2393-2404.	2.4	7
27	Spatial distribution of metals within the liver acinus and their perturbation by PCB126. Environmental Science and Pollution Research, 2018, 25, 16427-16433.	5.3	3
28	Trace Metal Imaging of Sulfate-Reducing Bacteria and Methanogenic Archaea at Single-Cell Resolution by Synchrotron X-Ray Fluorescence Imaging. Geomicrobiology Journal, 2018, 35, 81-89.	2.0	13
29	Intracellular in situ labeling of TiO2 nanoparticles for fluorescence microscopy detection. Nano Research, 2018, 11, 464-476.	10.4	30
30	Performance and Ongoing Development of the Velociprobe, a Fast Hard X-ray Nanoprobe for High-Resolution Ptychographic Imaging. Microscopy and Microanalysis, 2018, 24, 54-55.	0.4	13
31	Correlative 3D x-ray fluorescence and ptychographic tomography of frozen-hydrated green algae. Science Advances, 2018, 4, eaau4548.	10.3	79
32	Acetylation increases relative humidity threshold for ion transport in wood cell walls – A means to understanding decay resistance. International Biodeterioration and Biodegradation, 2018, 133, 230-237.	3.9	29
33	Zinc sparks induce physiochemical changes in the egg zona pellucida that prevent polyspermy. Integrative Biology (United Kingdom), 2017, 9, 135-144.	1.3	72
34	Synchrotron-based X-ray fluorescence microscopy enables multiscale spatial visualization of ions involved in fungal lignocellulose deconstruction. Scientific Reports, 2017, 7, 41798.	3.3	38
35	(Pentamethylcyclopentadienato)rhodium Complexes for Delivery of the Curcumin Anticancer Drug. European Journal of Inorganic Chemistry, 2017, 2017, 1812-1823.	2.0	16
36	Encapsulation, controlled release, and antitumor efficacy of cisplatin delivered in liposomes composed of sterol-modified phospholipids. European Journal of Pharmaceutical Sciences, 2017, 103, 85-93.	4.0	33

#	Article	IF	CITATIONS
37	Increased Throughput and Sensitivity of Synchrotron-Based Characterization for Photovoltaic Materials. IEEE Journal of Photovoltaics, 2017, 7, 763-771.	2.5	10
38	Imaging of Vanadium in Microfossils: A New Potential Biosignature. Astrobiology, 2017, 17, 1069-1076.	3.0	12
39	X-ray ptychographic and fluorescence microscopy of frozen-hydrated cells using continuous scanning. Scientific Reports, 2017, 7, 445.	3.3	88
40	Preserving elemental content in adherent mammalian cells for analysis by synchrotronâ€based xâ€ray fluorescence microscopy. Journal of Microscopy, 2017, 265, 81-93.	1.8	83
41	Microdistribution of lead in human teeth using microbeam synchrotron radiation X-ray fluorescence (μ-SRXRF). X-Ray Spectrometry, 2017, 46, 19-26.	1.4	6
42	Cementum structure in Beluga whale teeth. Acta Biomaterialia, 2017, 48, 289-299.	8.3	32
43	Intracellular distribution and stability of a luminescent rhenium(<scp>i</scp>) tricarbonyl tetrazolato complex using epifluorescence microscopy in conjunction with X-ray fluorescence imaging. Metallomics, 2017, 9, 382-390.	2.4	31
44	PlantPredict: Solar Performance Modeling Made Simple. , 2017, , .		3
45	X-ray fluorescence at nanoscale resolution for multicomponent layered structures: a solar cell caseÂstudy. Journal of Synchrotron Radiation, 2017, 24, 288-295.	2.4	27
46	Distribution of Iron Oxide Core-Titanium Dioxide Shell Nanoparticles in VX2 Tumor Bearing Rabbits Introduced by Two Different Delivery Modalities. Nanomaterials, 2016, 6, 143.	4.1	7
47	Directed plant cell-wall accumulation of iron: embedding co-catalyst for efficient biomass conversion. Biotechnology for Biofuels, 2016, 9, 225.	6.2	12
48	Carcinogenic Chromium(VI) Compounds Formed by Intracellular Oxidation of Chromium(III) Dietary Supplements by Adipocytes. Angewandte Chemie - International Edition, 2016, 55, 1742-1745.	13.8	54
49	Imaging trace element distributions in single organelles and subcellular features. Scientific Reports, 2016, 6, 21437.	3.3	39
50	Cell wall targeted <i>in planta</i> iron accumulation enhances biomass conversion and seed iron concentration in Arabidopsis and rice. Plant Biotechnology Journal, 2016, 14, 1998-2009.	8.3	19
51	Microplankton trace element contents: implications for mineral limitation of mesozooplankton in an HNLC area. Journal of Plankton Research, 2016, 38, 256-270.	1.8	13
52	HYBRID Simulations of Diffraction-Limited Focusing with Kirkpatrick-Baez Mirrors for a Next-Generation In Situ Hard X-ray Nanoprobe. Metallurgical and Materials Transactions A: Physical Metallurgy and Materials Science, 2016, 47, 5715-5721.	2.2	0
53	Micro X-ray Fluorescence Study of Late Pre-Hispanic Ceramics from the Western Slopes of the South Central Andes Region in the <i>Arica y Parinacota</i> Region, Chile: A New Methodological Approach. Applied Spectroscopy, 2016, 70, 1759-1769.	2.2	5
54	MicroXRF tomographic visualization of zinc and iron in the zebrafish embryo at the onset of the hatching period. Metallomics, 2016, 8, 1122-1130.	2.4	14

#	Article	lF	CITATIONS
55	Copper Uptake, Intracellular Localization, and Speciation in Marine Microalgae Measured by Synchrotron Radiation X-ray Fluorescence and Absorption Microspectroscopy. Environmental Science & Technology, 2016, 50, 8827-8839.	10.0	44
56	Copper, zinc and calcium: imaging and quantification in anterior pituitary secretory granules. Metallomics, 2016, 8, 1012-1022.	2.4	10
57	Endothelial Antioxidant-1: a Key Mediator of Copper-dependent Wound Healing in vivo. Scientific Reports, 2016, 6, 33783.	3.3	55
58	Advances and challenges in cryo ptychography at the Advanced Photon Source. AIP Conference Proceedings, 2016, 1696, .	0.4	0
59	2D/3D cryo x-ray fluorescence imaging at the bionanoprobe at the advanced photon source. AIP Conference Proceedings, 2016, , .	0.4	5
60	Carcinogenic Chromium(VI) Compounds Formed by Intracellular Oxidation of Chromium(III) Dietary Supplements by Adipocytes. Angewandte Chemie, 2016, 128, 1774-1777.	2.0	7
61	The â€~Tully monster' is a vertebrate. Nature, 2016, 532, 496-499.	27.8	35
62	The Bionanoprobe: Synchrotron-Based Hard X-ray Fluorescence Microscopy for 2D/3D Trace Element Mapping. Microscopy Today, 2015, 23, 26-29.	0.3	13
63	The inorganic anatomy of the mammalian preimplantation embryo and the requirement of zinc during the first mitotic divisions. Developmental Dynamics, 2015, 244, 935-947.	1.8	25
64	X-Ray Fluorescence Microscopy Demonstrates Preferential Accumulation of a Vanadium-Based Magnetic Resonance Imaging Contrast Agent in Murine Colonic Tumors. Molecular Imaging, 2015, 14, 7290.2015.00001.	1.4	10
65	Ultraviolet Germicidal Irradiation and Its Effects on Elemental Distributions in Mouse Embryonic Fibroblast Cells in X-Ray Fluorescence Microanalysis. PLoS ONE, 2015, 10, e0117437.	2.5	24
66	Cryogenic Sample Preparation Preserves Elemental Composition for Correlative Light and X-ray Fluorescence Microscopy. Microscopy and Microanalysis, 2015, 21, 877-878.	0.4	0
67	Simultaneous x-ray nano-ptychographic and fluorescence microscopy at the bionanoprobe. , 2015, , .		2
68	Opportunities and limitations for combined fly-scan ptychography and fluorescence microscopy. , 2015, 9592, .		2
69	Stacking multiple zone plates for efficient hard x-ray focusing at the Advanced Photon Source. Proceedings of SPIE, 2015, , .	0.8	0
70	Mechanisms of murine cerebral malaria: Multimodal imaging of altered cerebral metabolism and protein oxidation at hemorrhage sites. Science Advances, 2015, 1, e1500911.	10.3	25
71	Optimizing detector geometry for trace element mapping by X-ray fluorescence. Ultramicroscopy, 2015, 152, 44-56.	1.9	29
72	Simultaneous cryo X-ray ptychographic and fluorescence microscopy of green algae. Proceedings of the United States of America, 2015, 112, 2314-2319.	7.1	146

#	Article	IF	CITATIONS
73	Synchrotron-based X-ray Fluorescence Microscopy in Conjunction with Nanoindentation to Study Molecular-Scale Interactions of Phenol–Formaldehyde in Wood Cell Walls. ACS Applied Materials & Interfaces, 2015, 7, 6584-6589.	8.0	70
74	Continuous motion scan ptychography: characterization for increased speed in coherent x-ray imaging. Optics Express, 2015, 23, 5438.	3.4	102
75	IV Administered Gadodiamide Enters the Lumen of the Prostatic Glands: X-Ray Fluorescence Microscopy Examination of a Mouse Model. American Journal of Roentgenology, 2015, 205, W313-W319.	2.2	6
76	Metal contents of phytoplankton and labile particulate material in the North Atlantic Ocean. Progress in Oceanography, 2015, 137, 261-283.	3.2	81
77	Threshold for ion movements in wood cell walls below fiber saturation observed by X-ray fluorescence microscopy (XFM). Holzforschung, 2015, 69, 441-448.	1.9	36
78	Quantitative mapping of zinc fluxes in the mammalian egg reveals the origin of fertilization-induced zinc sparks. Nature Chemistry, 2015, 7, 130-139.	13.6	185
79	Metal-deficient aggregates and diminished copper found in cells expressing SOD1 mutations that cause ALS. Frontiers in Aging Neuroscience, 2014, 6, 110.	3.4	52
80	Non-negative matrix analysis for effective feature extraction in X-ray spectromicroscopy. Faraday Discussions, 2014, 171, 357-371.	3.2	37
81	Fresnel zone plate stacking in the intermediate field for high efficiency focusing in the hard X-ray regime. Optics Express, 2014, 22, 28142.	3.4	35
82	A Next-Generation Hard X-Ray Nanoprobe Beamline for In Situ Studies of Energy Materials and Devices. Metallurgical and Materials Transactions A: Physical Metallurgy and Materials Science, 2014, 45, 85-97.	2.2	14
83	XAS and XFM studies of selenium and copper speciation and distribution in the kidneys of selenite-supplemented rats. Metallomics, 2014, 6, 1602-1615.	2.4	30
84	Quantitation and localization of intracellular redox active metals by X-ray fluorescence microscopy in cortical neurons derived from APP and APLP2 knockout tissue. Metallomics, 2014, 6, 1894-1904.	2.4	21
85	3D imaging of transition metals in the zebrafish embryo by X-ray fluorescence microtomography. Metallomics, 2014, 6, 1648.	2.4	45
86	Scientific data exchange: a schema for HDF5-based storage of raw and analyzed data. Journal of Synchrotron Radiation, 2014, 21, 1224-1230.	2.4	86
87	Differential remineralization of major and trace elements in sinking diatoms. Limnology and Oceanography, 2014, 59, 689-704.	3.1	84
88	Wood as inspiration for new stimuli-responsive structures and materials. , 2014, , .		3
89	Multiscale deconstruction of molecular architecture in corn stover. Scientific Reports, 2014, 4, 3756.	3.3	30
90	Alignment of low-dose X-ray fluorescence tomographyÂimages using differential phase contrast. Journal of Synchrotron Radiation, 2014, 21, 229-234.	2.4	24

#	Article	IF	CITATIONS
91	The Bionanoprobe: hard X-ray fluorescence nanoprobe with cryogenic capabilities. Journal of Synchrotron Radiation, 2014, 21, 66-75.	2.4	151
92	Unsupervised cell identification on multidimensional X-ray fluorescence datasets. Journal of Synchrotron Radiation, 2014, 21, 568-579.	2.4	10
93	Opportunities in multidimensional trace metal imaging: taking copper-associated disease research to the next level. Analytical and Bioanalytical Chemistry, 2013, 405, 1809-1820.	3.7	35
94	Iron distribution through the developmental stages of Medicago truncatula nodules. Metallomics, 2013, 5, 1247.	2.4	52
95	Methylmercury Targets Photoreceptor Outer Segments. ACS Chemical Biology, 2013, 8, 2256-2263.	3.4	40
96	Epidermal Growth Factor Receptor Targeted Nuclear Delivery and High-Resolution Whole Cell X-ray Imaging of Fe ₃ O ₄ @TiO ₂ Nanoparticles in Cancer Cells. ACS Nano, 2013, 7, 10502-10517.	14.6	113
97	X-ray fluorescence imaging of single human cancer cells reveals that the N-heterocyclic ligands of iodinated analogues of ruthenium anticancer drugs remain coordinated after cellular uptake. Journal of Biological Inorganic Chemistry, 2013, 18, 845-853.	2.6	21
98	Trends in X-ray Fluorescence Microscopy. Synchrotron Radiation News, 2013, 26, 32-38.	0.8	17
99	Periplasmic response upon disruption of transmembrane Cu transport in Pseudomonas aeruginosa. Metallomics, 2013, 5, 144.	2.4	31
100	Tissue specific specialization of the nanoscale architecture of Arabidopsis. Journal of Structural Biology, 2013, 184, 103-114.	2.8	16
101	Intracellular Targeting and Pharmacological Activity of the Superoxide Dismutase Mimics MnTE-2-PyP ⁵⁺ and MnTnHex-2-PyP ⁵⁺ Regulated by Their Porphyrin Ring Substituents. Inorganic Chemistry, 2013, 52, 4121-4123.	4.0	27
102	A next-generation in-situ nanoprobe beamline for the Advanced Photon Source. Proceedings of SPIE, 2013, , .	0.8	2
103	Sub-100-nm 3D-elemental mapping of frozen-hydrated cells using the bionanoprobe. Proceedings of SPIE, 2013, , .	0.8	0
104	Optomechanical design of a modular K-B mirror mount system for x-ray microfocusing at the advanced photon source. , 2013, , .		3
105	Synchrotron X-ray fluorescence studies of a bromine-labelled cyclic RCD peptide interacting with individual tumor cells. Journal of Synchrotron Radiation, 2013, 20, 226-233.	2.4	10
106	Role of biogenic silica in the removal of iron from the Antarctic seas. Nature Communications, 2013, 4, 1981.	12.8	61
107	Three-dimensional Imaging of Crystalline Inclusions Embedded in Intact Maize Stalks. Scientific Reports, 2013, 3, 2843.	3.3	4
108	Rapid and Accurate Analysis of an X-Ray Fluorescence Microscopy Data Set through Gaussian Mixture-Based Soft Clustering Methods. Microscopy and Microanalysis, 2013, 19, 1281-1289.	0.4	14

#	Article	IF	CITATIONS
109	Mapping the subcellular localization of Fe ₃ O ₄ @TiO ₂ nanoparticles by X-ray Fluorescence Microscopy. Journal of Physics: Conference Series, 2013, 463, 012020.	0.4	4
110	New Developments in Hard X-ray Fluorescence Microscopy for In-situ Investigations of Trace Element Distributions in Aqueous Systems of Soil Colloids. Journal of Physics: Conference Series, 2013, 463, 012005.	0.4	2
111	Selenium Metabolism in Cancer Cells: The Combined Application of XAS and XFM Techniques to the Problem of Selenium Speciation in Biological Systems. Nutrients, 2013, 5, 1734-1756.	4.1	60
112	Simultaneous X-ray fluorescence and ptychographic microscopy of Cyclotella meneghiniana. Optics Express, 2012, 20, 18287.	3.4	75
113	Role of Copper Transport Protein Antioxidant 1 in Angiotensin Il–Induced Hypertension. Hypertension, 2012, 60, 476-486.	2.7	57
114	X-Ray Fluorescence Microscopy for Investigation of Archival Tissues. Health Physics, 2012, 103, 181-186.	0.5	25
115	Submicron hard X-ray fluorescence imaging of synthetic elements. Analytica Chimica Acta, 2012, 722, 21-28.	5.4	7
116	Significant silicon accumulation by marine picocyanobacteria. Nature Geoscience, 2012, 5, 886-891.	12.9	96
117	Identifying metalloproteins through X-ray fluorescence mapping and mass spectrometry. Metallomics, 2012, 4, 921.	2.4	22
118	High-Resolution Imaging of Selenium in Kidneys: A Localized Selenium Pool Associated with Glutathione Peroxidase 3. Antioxidants and Redox Signaling, 2012, 16, 185-192.	5.4	44
119	Role of diatoms in nickel biogeochemistry in the ocean. Global Biogeochemical Cycles, 2012, 26, .	4.9	58
120	The Unique Biogeochemical Signature of the Marine Diazotroph Trichodesmium. Frontiers in Microbiology, 2012, 3, 150.	3.5	57
121	Nanocarriers Enhance Doxorubicin Uptake in Drug-Resistant Ovarian Cancer Cells. Cancer Research, 2012, 72, 769-778.	0.9	97
122	Synchrotron radiation induced X-ray emission studies of the antioxidant mechanism of the organoselenium drug ebselen. Journal of Biological Inorganic Chemistry, 2012, 17, 589-598.	2.6	16
123	LOCALIZATION OF IRON WITHIN CENTRIC DIATOMS OF THE GENUS <i>THALASSIOSIRA</i> ¹ . Journal of Phycology, 2012, 48, 626-634.	2.3	37
124	Uptake, Distribution, and Speciation of Selenoamino Acids by Human Cancer Cells: X-ray Absorption and Fluorescence Methods. Biochemistry, 2011, 50, 1641-1650.	2.5	50
125	Direct Determination of the Intracellular Oxidation State of Plutonium. Inorganic Chemistry, 2011, 50, 7591-7597.	4.0	15
126	Metabolism of Selenite in Human Lung Cancer Cells: X-Ray Absorption and Fluorescence Studies. Journal of the American Chemical Society, 2011, 133, 18272-18279.	13.7	73

#	Article	IF	CITATIONS
127	Uptake and Distribution of a Platinum(II)-Carborane Complex Within a Tumour Cell Using Synchrotron XRF Imaging. Australian Journal of Chemistry, 2011, 64, 253.	0.9	10
128	Plutonium uptake and distribution in mammalian cells: Molecular vs. polymeric plutonium. International Journal of Radiation Biology, 2011, 87, 1023-1032.	1.8	18
129	Zinc Sparks Are Triggered by Fertilization and Facilitate Cell Cycle Resumption in Mammalian Eggs. ACS Chemical Biology, 2011, 6, 716-723.	3.4	184
130	Increased brain iron coincides with early plaque formation in a mouse model of Alzheimer's disease. NeuroImage, 2011, 55, 32-38.	4.2	123
131	Distribution and speciation of gold in biogenic and abiogenic calcium carbonates – Implications for the formation of gold anomalous calcrete. Geochimica Et Cosmochimica Acta, 2011, 75, 1942-1956.	3.9	28
132	Elemental composition of equatorial Pacific diatoms exposed to additions of silicic acid and iron. Deep-Sea Research Part II: Topical Studies in Oceanography, 2011, 58, 512-523.	1.4	37
133	Metal quotas of plankton in the equatorial Pacific Ocean. Deep-Sea Research Part II: Topical Studies in Oceanography, 2011, 58, 325-341.	1.4	103
134	Selectivity in biomineralization of barium and strontium. Journal of Structural Biology, 2011, 176, 192-202.	2.8	53
135	Elemental Profiling of Single Bacterial Cells As a Function of Copper Exposure and Growth Phase. PLoS ONE, 2011, 6, e21255.	2.5	10
136	Hard X-ray Fluorescence Microscopy to Determine the Element Distribution of Soil Colloids in Aqueous Environment. , 2011, , .		2
137	PAST AND FUTURE WORK ON RADIOBIOLOGY MEGA-STUDIES: A CASE STUDY AT ARGONNE NATIONAL LABORATORY. Health Physics, 2011, 100, 613-621.	0.5	23
138	Spatially Resolved Sulfur Speciation in Urban Soils. , 2011, , .		2
139	Interrogation of EGFR-Targeted Uptake of TiO[sub 2] Nanoconjugates by X-ray Fluorescence Microscopy. , 2011, 1365, 423-426.		4
140	Combined X-ray Microfluorescence and Atomic Force Microscopy Studies of Mg Distribution in Whole Cells. , 2011, , .		0
141	Radiation damage to protein crystals is reduced with a micron-sized X-ray beam. Acta Crystallographica Section A: Foundations and Advances, 2011, 67, C158-C158.	0.3	0
142	A Multimodal Nanocomposite for Biomedical Imaging. AIP Conference Proceedings, 2011, 1365, 379.	0.4	5
143	Intracellular concentration map of magnesium in whole cells by combined use of X-ray fluorescence microscopy and atomic force microscopy. Spectrochimica Acta, Part B: Atomic Spectroscopy, 2011, 66, 834-840.	2.9	20
144	Quantitative comparison of preparation methodologies for x-ray fluorescence microscopy of brain tissue. Analytical and Bioanalytical Chemistry, 2011, 401, 853-864.	3.7	53

#	Article	IF	CITATIONS
145	<i>^î²</i> â€Cell subcellular localization of glucoseâ€stimulated Mn uptake by Xâ€ray fluorescence microscopy: implications for pancreatic MRI. Contrast Media and Molecular Imaging, 2011, 6, 474-481.	0.8	16
146	Selective Sequestration of Strontium in Desmid Green Algae by Biogenic Coâ€precipitation with Barite. ChemSusChem, 2011, 4, 470-473.	6.8	37
147	Calcium-dependent copper redistributions in neuronal cells revealed by a fluorescent copper sensor and X-ray fluorescence microscopy. Proceedings of the National Academy of Sciences of the United States of America, 2011, 108, 5980-5985.	7.1	182
148	Reduced Utilization of Selenium by Naked Mole Rats Due to a Specific Defect in GPx1 Expression. Journal of Biological Chemistry, 2011, 286, 17005-17014.	3.4	35
149	An iron-dependent and transferrin-mediated cellular uptake pathway for plutonium. Nature Chemical Biology, 2011, 7, 560-565.	8.0	76
150	Radiation damage in protein crystals is reduced with a micron-sized X-ray beam. Proceedings of the National Academy of Sciences of the United States of America, 2011, 108, 6127-6132.	7.1	124
151	Variations in <i>Synechococcus</i> cell quotas of phosphorus, sulfur, manganese, iron, nickel, and zinc within mesoscale eddies in the Sargasso Sea. Limnology and Oceanography, 2010, 55, 492-506.	3.1	35
152	One-Micron Beams for Macromolecular Crystallography at GMâ^•CA-CAT. , 2010, , .		9
153	Biomedical applications of X-ray absorption and vibrational spectroscopic microscopies in obtaining structural information from complex systems. Radiation Physics and Chemistry, 2010, 79, 176-184.	2.8	34
154	Virulence-related Mycobacterium avium subsp hominissuis MAV_2928 gene is associated with vacuole remodeling in macrophages. BMC Microbiology, 2010, 10, 100.	3.3	29
155	Selective Aggregation of a Platinum–Gadolinium Complex Within a Tumorâ€Cell Nucleus. Angewandte Chemie - International Edition, 2010, 49, 1231-1233.	13.8	44
156	Quantification of phosphorus in single cells using synchrotron X-ray fluorescence. Journal of Synchrotron Radiation, 2010, 17, 560-566.	2.4	33
157	Zinc availability regulates exit from meiosis in maturing mammalian oocytes. Nature Chemical Biology, 2010, 6, 674-681.	8.0	208
158	Zernike phase contrast in scanning microscopy with X-rays. Nature Physics, 2010, 6, 883-887.	16.7	105
159	X-Ray Fluorescence Microscopy Reveals Accumulation and Secretion of Discrete Intracellular Zinc Pools in the Lactating Mouse Mammary Gland. PLoS ONE, 2010, 5, e11078.	2.5	52
160	Quantitative 3D elemental microtomography of <i>Cyclotella meneghiniana</i> at 400-nm resolution. Proceedings of the National Academy of Sciences of the United States of America, 2010, 107, 15676-15680.	7.1	146
161	Unexpected Role of the Copper Transporter ATP7A in PDGF-Induced Vascular Smooth Muscle Cell Migration. Circulation Research, 2010, 107, 787-799.	4.5	73
162	Wilson Disease at a Single Cell Level. Journal of Biological Chemistry, 2010, 285, 30875-30883.	3.4	95

#	Article	IF	CITATIONS
163	Imaging Metals in Proteins by Combining Electrophoresis with Rapid X-ray Fluorescence Mapping. ACS Chemical Biology, 2010, 5, 577-587.	3.4	52
164	Hard X-ray fluorescence tomography—an emerging tool for structural visualization. Current Opinion in Structural Biology, 2010, 20, 606-614.	5.7	153
165	Uptake and Distribution of Ultrasmall Anatase TiO ₂ Alizarin Red S Nanoconjugates in <i>Arabidopsis thaliana</i> . Nano Letters, 2010, 10, 2296-2302.	9.1	395
166	Silicon nitride as a versatile growth substrate for microspectroscopic imaging and mapping of individual cells. Molecular BioSystems, 2010, 6, 1316.	2.9	72
167	Loss of Pluripotency in Human Embryonic Stem Cells Directly Correlates with an Increase in Nuclear Zinc. PLoS ONE, 2010, 5, e12308.	2.5	18
168	Variations in Synechococcus cell quotas of phosphorus, sulfur, manganese, iron, nickel, and zinc within mesoscale eddies in the Sargasso Sea. Limnology and Oceanography, 2010, 55, 492-506.	3.1	30
169	Uptake mechanisms of EGFR-targeted TiO2 nanoparticles Journal of Clinical Oncology, 2010, 28, e13583-e13583.	1.6	0
170	Ductal Carcinoma in Situ: X-ray Fluorescence Microscopy and Dynamic Contrast-enhanced MR Imaging Reveals Gadolinium Uptake within Neoplastic Mammary Ducts in a Murine Model. Radiology, 2009, 253, 399-406.	7.3	76
171	Biological applications of X-ray microprobes. International Journal of Radiation Biology, 2009, 85, 710-713.	1.8	12
172	Labeling TiO ₂ Nanoparticles with Dyes for Optical Fluorescence Microscopy and Determination of TiO ₂ –DNA Nanoconjugate Stability. Small, 2009, 5, 1318-1325.	10.0	95
173	Response to Guzzi & Pigatto'sComments onMigration of mercury from dental amalgam through human teethby H. H. Harriset al.(2008).J. Synchrotron Rad.15, 123–128. Journal of Synchrotron Radiation, 2009, 16, 437-438.	2.4	1
174	COPPER AND ANGIOGENESIS: UNRAVELLING A RELATIONSHIP KEY TO CANCER PROGRESSION. Clinical and Experimental Pharmacology and Physiology, 2009, 36, 88-94.	1.9	251
175	Multiple protective activities of neuroglobin in cultured neuronal cells exposed to hypoxia reâ€oxygenation injury. Journal of Neurochemistry, 2009, 108, 1143-1154.	3.9	63
176	Mechanisms of gold biomineralization in the bacterium <i>Cupriavidus metallidurans</i> . Proceedings of the United States of America, 2009, 106, 17757-17762.	7.1	283
177	X-Ray Fluorescence Microscopy Reveals the Role of Selenium in Spermatogenesis. Journal of Molecular Biology, 2009, 389, 808-818.	4.2	65
178	Quantitative scanning differential phase contrast microscopy. Journal of Physics: Conference Series, 2009, 186, 012006.	0.4	3
179	Characterization of phosphorus, calcium, iron, and other elements in organisms at subâ€micron resolution using Xâ€ray fluorescence spectromicroscopy. Limnology and Oceanography: Methods, 2009, 7, 42-51.	2.0	23
180	A link between copper and dental caries in human teeth identified by X-ray fluorescence elemental mapping. Journal of Biological Inorganic Chemistry, 2008, 13, 303-306.	2.6	35

#	Article	IF	CITATIONS
181	Migration of mercury from dental amalgam through human teeth. Journal of Synchrotron Radiation, 2008, 15, 123-128.	2.4	37
182	Differential phase contrast with a segmented detector in a scanning X-ray microprobe. Journal of Synchrotron Radiation, 2008, 15, 355-362.	2.4	75
183	Highâ€resolution Xâ€ray imaging of <i>Plasmodium falciparum</i> â€infected red blood cells. Cytometry Part A: the Journal of the International Society for Analytical Cytology, 2008, 73A, 949-957.	1.5	49
184	Gadolinium-conjugated TiO2-DNA oligonucleotide nanoconjugates show prolonged intracellular retention period and T1-weighted contrast enhancement in magnetic resonance images. Nanomedicine: Nanotechnology, Biology, and Medicine, 2008, 4, 201-207.	3.3	46
185	Quantitative Phase Imaging with a Scanning Transmission X-Ray Microscope. Physical Review Letters, 2008, 100, 163902.	7.8	93
186	Exploring Ocean Biogeochemistry by Single ell Microprobe Analysis of Protist Elemental Composition ¹ . Journal of Eukaryotic Microbiology, 2008, 55, 151-162.	1.7	34
187	Cell-Permeable MR Contrast Agents with Increased Intracellular Retention. Bioconjugate Chemistry, 2008, 19, 2049-2059.	3.6	51
188	Synthesis, Characterization, and <i>in Vitro</i> Testing of Superparamagnetic Iron Oxide Nanoparticles Targeted Using Folic Acid-Conjugated Dendrimers. ACS Nano, 2008, 2, 773-783.	14.6	163
189	Probing radiation damage with a 1-micron beam. Acta Crystallographica Section A: Foundations and Advances, 2008, 64, C179-C180.	0.3	0
190	Microprobe XRF Mapping and XAS Investigations of the Intracellular Metabolism of Arsenic for Understanding Arsenic-Induced Toxicity. Chemical Research in Toxicology, 2008, 21, 1760-1769.	3.3	49
191	Focusing of hard x-rays to 16 nanometers with a multilayer Laue lens. Applied Physics Letters, 2008, 92, 221114.	3.3	190
192	Mechanism of Selenium-Induced Inhibition of Arsenic-Enhanced UVR Carcinogenesis in Mice. Environmental Health Perspectives, 2008, 116, 703-708.	6.0	23
193	Levels of Zinc, Selenium, Calcium, and Iron in Benign Breast Tissue and Risk of Subsequent Breast Cancer. Cancer Epidemiology Biomarkers and Prevention, 2007, 16, 1682-1685.	2.5	113
194	Beamline Design for a BioNanoprobe: Stability and Coherence. AIP Conference Proceedings, 2007, , .	0.4	1
195	Optomechanical Design of a Hard X-ray Nanoprobe Instrument with Nanometer-Scale Active Vibration Control. AIP Conference Proceedings, 2007, , .	0.4	17
196	Epitaxial growth of (FeCo)[sub x]Ge[sub 1â^'x](001). Journal of Vacuum Science & Technology B, 2007, 25, 1217.	1.3	4
197	Takagi-Taupin description of x-ray dynamical diffraction from diffractive optics with large numerical aperture. Physical Review B, 2007, 76, .	3.2	128
198	X-ray fluorescence microscopy reveals large-scale relocalization and extracellular translocation of cellular copper during angiogenesis. Proceedings of the National Academy of Sciences of the United States of America, 2007, 104, 2247-2252.	7.1	178

#	Article	IF	CITATIONS
199	X-Ray Spectromicroscopy—A Tool for Environmental Sciences. Environmental Science & Technology, 2007, 41, 6885-6889.	10.0	70
200	Intracellular Distribution of TiO2â DNA Oligonucleotide Nanoconjugates Directed to Nucleolus and Mitochondria Indicates Sequence Specificity. Nano Letters, 2007, 7, 596-601.	9.1	116
201	DNAâ^'TiO2 Nanoconjugates Labeled with Magnetic Resonance Contrast Agents. Journal of the American Chemical Society, 2007, 129, 15760-15761.	13.7	105
202	Combinatorial synthesis and characterization of a ternary epitaxial film of Co and Mn doped Ge (001). Applied Surface Science, 2007, 254, 709-713.	6.1	13
203	A robot-based detector manipulator system for a hard X-ray nanoprobe instrument. Nuclear Instruments and Methods in Physics Research, Section A: Accelerators, Spectrometers, Detectors and Associated Equipment, 2007, 582, 159-161.	1.6	10
204	A method for phase reconstruction from measurements obtained using a configured detector with a scanning transmission X-ray microscope. Nuclear Instruments and Methods in Physics Research, Section A: Accelerators, Spectrometers, Detectors and Associated Equipment, 2007, 582, 218-220.	1.6	8
205	Selective x-ray Bragg spectrometry: optimizing fluorescence microprobe sensitivity for precious metals. X-Ray Spectrometry, 2007, 36, 111-121.	1.4	3
206	The application of synchrotron radiation induced X-ray emission in the measurement of zinc and lead in Wistar rat ameloblasts. Archives of Oral Biology, 2007, 52, 938-944.	1.8	12
207	Nanoparticles for Applications in Cellular Imaging. Nanoscale Research Letters, 2007, 2, 430-41.	5.7	158
208	THE OXIDATION STATE OF EUROPIUM IN HYDROTHERMAL SCHEELITE: IN SITU MEASUREMENT BY XANES SPECTROSCOPY. Canadian Mineralogist, 2006, 44, 1079-1087.	1.0	17
209	Nanometer Linear Focusing of Hard X Rays by a Multilayer Laue Lens. Physical Review Letters, 2006, 96, 127401.	7.8	257
210	210 Development of titanium dioxide-DNA nanocomposites for intracellular delivery and radiation-mediated dna scission. Radiotherapy and Oncology, 2006, 78, S73-S74.	0.6	0
211	Elemental analysis of the Mycobacterium avium phagosome in Balb/c mouse macrophages. Biochemical and Biophysical Research Communications, 2006, 344, 1346-1351.	2.1	27
212	Regulatory properties and cellular redistribution of zinc during macrophage differentiation of human leukemia cells. Journal of Structural Biology, 2006, 155, 2-11.	2.8	34
213	Correlative microXRF and optical immunofluorescence microscopy of adherent cells labeled with ultrasmall gold particles. Journal of Structural Biology, 2006, 155, 22-29.	2.8	84
214	Intracellular distributions of essential elements in cardiomyocytes. Journal of Structural Biology, 2006, 155, 12-21.	2.8	32
215	Quantitative Imaging of Cell-Permeable Magnetic Resonance Contrast Agents Using X-Ray Fluorescence. Molecular Imaging, 2006, 5, 7290.2006.00026.	1.4	32
216	Structure and magnetism of Coa(1â^`x)MnaxGeb epitaxial films. Applied Surface Science, 2006, 252, 2512-2517.	6.1	8

#	Article	IF	CITATIONS
217	X-ray fluorescence microprobe imaging in biology and medicine. Journal of Cellular Biochemistry, 2006, 99, 1489-1502.	2.6	213
218	Quantitative imaging of cell-permeable magnetic resonance contrast agents using x-ray fluorescence. Molecular Imaging, 2006, 5, 485-97.	1.4	17
219	Investigation of Fly Ash Particulates Using SEM, TEM and Synchrotron Microprobe Techniques. Microscopy and Microanalysis, 2005, 11, .	0.4	1
220	Mapping 3D X-ray Fluorescence Datasets to Elemental Distributions using Principal Component Analysis and Fitting. Microscopy and Microanalysis, 2005, 11, .	0.4	2
221	PIXE Real-Time Quantitative Image Projection Applied to Synchrotron XRF Imaging using the X-ray Fluorescence Microprobe. Microscopy and Microanalysis, 2005, 11, .	0.4	2
222	Nuclear microprobe – synchrotron synergy: Towards integrated quantitative real-time elemental imaging using PIXE and SXRF. Nuclear Instruments & Methods in Physics Research B, 2005, 231, 183-188.	1.4	129
223	Cluster analysis in soft X-ray spectromicroscopy: Finding the patterns in complex specimens. Journal of Electron Spectroscopy and Related Phenomena, 2005, 144-147, 1137-1143.	1.7	74
224	Zinc Concentration in Esophageal Biopsy Specimens Measured by X-Ray Fluorescence and Esophageal Cancer Risk. Journal of the National Cancer Institute, 2005, 97, 301-306.	6.3	153
225	Changes of the phagosomal elemental concentrations by Mycobacterium tuberculosis Mramp. Microbiology (United Kingdom), 2005, 151, 323-332.	1.8	47
226	Imaging of the intracellular topography of copper with a fluorescent sensor and by synchrotron x-ray fluorescence microscopy. Proceedings of the National Academy of Sciences of the United States of America, 2005, 102, 11179-11184.	7.1	351
227	Self-Assembled, Mesoporous Polymeric Networks for Patterned Protein Arrays. Langmuir, 2005, 21, 10301-10306.	3.5	17
228	Conceptual Design For A Beamline For A Hard x-ray Nanoprobe with 30 nm Spatial Resolution. AlP Conference Proceedings, 2004, , .	0.4	7
229	Design for an X-ray Nanoprobe Prototype with a Sub-10-nm Positioning Requirement. AIP Conference Proceedings, 2004, , .	0.4	1
230	Fast Differential Phase-Contrast Imaging and Total Fluorescence Yield Mapping in a Hard X-ray Fluorescence Microprobe. AIP Conference Proceedings, 2004, , .	0.4	7
231	Evidence for strain compensation in stabilizing epitaxial growth of highly doped germanium. Physical Review B, 2004, 69, .	3.2	27
232	Multilayer Laue lenses as high-resolution x-ray optics. , 2004, 5539, 185.		58
233	Composition characterization of combinatorial materials by scanning X-ray fluorescence microscopy using microfocused synchrotron X-ray beam. Applied Surface Science, 2004, 223, 214-219.	6.1	23
234	Structural investigation of CoMnGe combinatorial epitaxial thin films using microfocused synchrotron X-ray. Applied Surface Science, 2004, 223, 175-182.	6.1	17

#	Article	IF	CITATIONS
235	Cluster analysis of soft X-ray spectromicroscopy data. Ultramicroscopy, 2004, 100, 35-57.	1.9	180
236	Tapered tilted linear zone plates for focusing hard x-rays. , 2004, , .		4
237	The evolution of hard x-ray tomography from the micrometer to the nanometer length scale. , 2004, , .		3
238	Biology of TiO2–oligonucleotide nanocomposites. Nature Materials, 2003, 2, 343-346.	27.5	286
239	Quantifying Trace Elements in Individual Aquatic Protist Cells with a Synchrotron X-ray Fluorescence Microprobe. Analytical Chemistry, 2003, 75, 3806-3816.	6.5	216
240	Data analysis for X-ray fluorescence imaging. European Physical Journal Special Topics, 2003, 104, 617-622.	0.2	26
241	High resolution X-ray tomography with applications in biology and materials science. European Physical Journal Special Topics, 2003, 104, 607-613.	0.2	5
242	MAPS : A set of software tools for analysis and visualization of 3D X-ray fluorescence data sets. European Physical Journal Special Topics, 2003, 104, 635-638.	0.2	147
243	The 2-ID-B intermediate-energy scanning X-ray microscope at the APS. European Physical Journal Special Topics, 2003, 104, 11-15.	0.2	24
244	Intracellular localization of titanium dioxide-biomolecule nanocomposites. European Physical Journal Special Topics, 2003, 104, 317-319.	0.2	4
245	Cluster analysis of soft X-ray spectromicroscopy data. European Physical Journal Special Topics, 2003, 104, 623-626.	0.2	10
246	COMPUTED TOMOGRAPHY OF CRYOGENIC CELLS. Surface Review and Letters, 2002, 09, 177-183.	1.1	57
247	Nanotomography of labeled cryogenic cells. , 2002, 4503, 156.		1
248	Tomographic imaging of biological specimens with the cryo transmission X-ray microscope. Nuclear Instruments and Methods in Physics Research, Section A: Accelerators, Spectrometers, Detectors and Associated Equipment, 2001, 467-468, 1308-1311.	1.6	21
249	Visualizing specific nuclear proteins in eukaryotic cells using soft X-ray microscopy. Nuclear Instruments and Methods in Physics Research, Section A: Accelerators, Spectrometers, Detectors and Associated Equipment, 2001, 467-468, 1312-1314.	1.6	1
250	Dark field X-ray microscopy: the effects of condenser/detector aperture. Ultramicroscopy, 2001, 87, 25-44.	1.9	23
251	X-ray microscopic studies of labeled nuclear cell structures. AIP Conference Proceedings, 2000, , .	0.4	2
252	X-Ray Microscopic Studies of the Drosophila Dosage Compensation Complex. Journal of Structural Biology, 2000, 132, 123-132.	2.8	44

#	Article	IF	CITATIONS
253	A shutter–photodiode combination for UV and soft X-ray beamlines. Journal of Synchrotron Radiation, 1999, 6, 50-50.	2.4	16